Acceptor Decoration of Threading Dislocations in (Al, Ga)N/GaN Heterostructures

Rong Wang[1,2,*] Xiaodong Tong,[1,2] Jianxing Xu,[1,2] Chenglong Dong,[1,2] Zhe Cheng,[3,4] Lian Zhang,[3,4] Shiyong Zhang,[1,2] Penghui Zheng,[1,2] Feng-Xiang Chen,[5] Yun Zhang,[3,4] and Wei Tan[1,2,†]

[1]*Microsystem and Terahertz Research Center, China Academy of Engineering Physics, Chengdu, 610200 Sichuan, China*

[2]*Institute of Electronic Engineering, China Academy of Engineering Physics, Mianyang, 621999 Sichuan, China*

[3]*Institute of Semiconductors, Chinese Academy of Sciences, 100083 Beijing, China*

[4]*University of Chinese Academy of Sciences, 100049 Beijing, China*

[5]*Department of Physics, School of Science and Technology, Wuhan University of Technology, Wuhan, 430070 Hubei, China*

We demonstrate that threading dislocations in (Al, Ga)N/GaN heterostructures can be spontaneously decorated by acceptors during the epitaxial process. First-principles calculations show that the threading dislocation introduces detrimental deep electronic states both above the valence-band maximum (VBM) and below the conduction-band minimum (CBM) of GaN. Because of the electron transfer between the occupied level above the VBM of the threading dislocation and the defect states of acceptors, acceptors will decorate the threading dislocation, which leads to the shift of the dislocation states. For the occupied deep states above the VBM, the acceptor decoration shifts the deep states toward the VBM, which may constructively contribute to the dislocation tolerance of (Al, Ga)N/GaN heterostructures. For the unoccupied states below the CBM, the acceptor-decorated dislocation provides an additional electron-transfer channel besides that through the pure threading dislocations. These two distinct electron-transfer channels are observed in reverse-biased (Al, Ga)N/GaN Schottky diodes, which is characterized by two distinct Frenkel-Poole-emission states.

I. INTRODUCTION

(Al, Ga)N/GaN heterostructures hold great promise in high-temperature, high-frequency, and high-power applications because of their excellent properties such as the wide band gap, high breakdown fields, high saturation electron drift velocity, and strong polarization [1–3]. During the epitaxy of (Al, Ga)N/GaN heterostructures, a high density of dislocations occurs because of thermal and lattice mismatch between GaN and its substrates [4,5]. In common semiconductors, dislocation introduces deep levels in the band gap, gives rise to nonradiative recombination, and degrades the electronic and optical properties of semiconductors [6,7]. However, (Al, Ga)N/GaN heterostructures exhibit excellent dislocation tolerance. Even though the density of dislocations ranges from 10^7 to 10^{11} cm^{-2} [8], (Al, Ga)N/GaN heterostructures have shown great success in applications such as light-emitting diodes, laser diodes, Schottky-barrier diodes, and high-electron-mobility transistors [9–11].

Previous studies showed that dislocations in GaN and its heterostructures are mainly threading dislocations [12]. For (Al, Ga)N/GaN heterostructures, the density and thus the effect of threading edge dislocations are greater than those of threading screw or mixed dislocations [13,14]. Therefore, we concentrate on the effect of threading edge dislocations on the properties of (Al, Ga)N/GaN heterostructures. The dominant geometric structure for threading edge dislocations is the 5-7-atom-ring-core structure, which has been verified by both theoretical studies and transmission electron microscopy [15,16]. It was demonstrated that the 5-7-atom-ring dislocation introduces deep-level states in the band gap of gallium nitrides [17–19]. These deep-level states serve as nonradiative recombination centers, which would deteriorate the performance of GaN-based devices.

Recent work showed that from the point of view of strain relaxation, the threading dislocation could interact with interstitial oxygen atoms (O_i) to lower the formation energy of oxygen due to the steric effect [20]. The oxygen passivation eliminates the deep-level states of threading dislocations, which could be beneficial for GaN devices. However, the O_i-passivation process happens

---

*wangrong@mtrc.ac.cn
†tanwei@mtrc.ac.cn

only in the nonequilibrium regime, where the formation of substitutional oxygen at the N site (O_N) at the dislocation core is kinetically prohibited and the Ga supply must be removed [20]. This situation does not commonly occur during the epitaxy of gallium nitrides. The interaction of defects in semiconductors is determined not only by the steric effect but also by the electronic effect [6]. The electronic effect between defects has been studied in GaAs [6], ZnO [21], and diamond [22], and exhibits the capability of lowering defect-formation energies and changing defect-level positions in the band gap. However, the electronic effect between point defects and dislocations in GaN and its impact on GaN devices has been rarely studied.

In this work, we investigate the electronic interaction between acceptors and threading dislocations in (Al, Ga)N/GaN heterostructures. First-principles calculations indicate that pure threading dislocations introduce deep occupied states above the valence-band maximum (VBM) and unoccupied deep states below the conduction-band minimum (CBM). Because of the electron transfer between the occupied state of the threading dislocation and defect levels of acceptors, the acceptor decoration shifts the detrimental deep electronic state of threading dislocations toward the VBM. This eliminates the deep-level states of pure threading dislocations, which may constructively contribute to the dislocation tolerance of GaN devices. On the other hand, the unoccupied state below the CBM provides an additional electron-transfer channel besides that through the pure threading dislocation. These two channels can lead to two distinct Frenkel-Poole- (FP) emission states in (Al, Ga)N/GaN devices.

II. THEORETICAL DESCRIPTION

Figure 1 displays the atomic structure of the threading dislocation investigated in this work. The 5-7-atom-ring-core structure of the threading dislocation is modeled within a 1.7-nm GaN nanorod with 108 Ga and N atoms
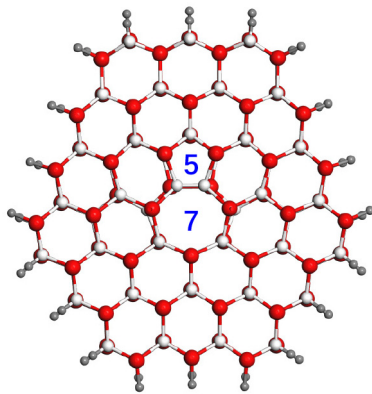
FIG. 1. Optimized atomic structure of the 5-7-atom-ring-core threading dislocation. Ga, N, and H atoms are denoted by red, white, and gray balls, respectively.

inside a periodic supercell of 5×5 nm^2. The dangling bonds of Ga and N atoms at the edges of the nanorod are passivated by pseudohydrogen atoms with 1.25 and 0.75 electrons, respectively.

First-principles calculations are performed with projector-augmented-wave pseudopotentials as implemented in the Vienna *ab initio* simulation package [23,24]. The Ga 3d states are included as valence electrons in the pseudopotentials. Plane-wave cutoff energies are set as 350 eV. The structural relaxation is performed by the generalized-gradient approximation formulated by Perdew, Burke, and Ernzerhof. During electronic calculations, the hybrid density functional proposed by Heyd, Scuseria, and Ernzerhof (HSE06) is used [25]. The atomic structures are optimized until the changes in total energy are less than 1×10^{-5} eV per cell. The Monkhorst-Pack scheme with a Γ-centered $1 \times 1 \times 5$ special k-point mesh is used to sample the reciprocal space of the supercell [26].

III. RESULTS AND DISCUSSION

A. Properties of dislocations in GaN

We first calculate the density of states for the pure threading dislocation to investigate its electronic properties. As shown in Fig. 2(b), the deep states of the pure threading dislocation both above the VBM and below the CBM of GaN. The 5-7-atom-ring core is characterized by the formation of alternating Ga-Ga dimers and N-N dimers along the dislocation line (Fig. 1). These dimers play important roles in the electronic properties of the threading dislocation. The dangling bonds of Ga and N atoms nominally have 0.75 and 1.25 electrons, respectively. The bonding states of the Ga-Ga dimer are filled with $(0.75) \times 2 = 1.5$ electrons and the antibonding state is empty. For N-N dimers, two of the $(1.25) \times 2 = 2.5$ electrons occupy the bonding state, and the remaining 0.5 electrons occupy the antibonding state [Fig. 3(a)]. On structural reconstruction, electron transfer occurs from the antibonding states of N-N dimers to the bonding states of Ga-Ga dimers and gives rise to the occupied bonding state of the 5-7-atom-ring-core dislocation [Fig. 3(a)].

To verify the origin of the occupied defect level of the pure 5-7-atom-ring-core threading dislocation, we calculate the charge density isosurface of the occupied deep level above the VBM. As shown in Fig. 3(b), the occupied states above the VBM mostly originate from the Ga-Ga dimer at the dislocation core, which is consistent with the electron-transfer model as shown in Fig. 3(a). Because of the formation of Ga-Ga dimers, the bonding between Ga and its nearest neighboring N atoms is affected. Therefore, N atoms that connect with Ga-Ga dimers at the dislocation core also partially contribute to the formation of the occupied states above the VBM of GaN.

Because the defect level of the threading dislocation above the VBM is fully occupied, the dislocation will
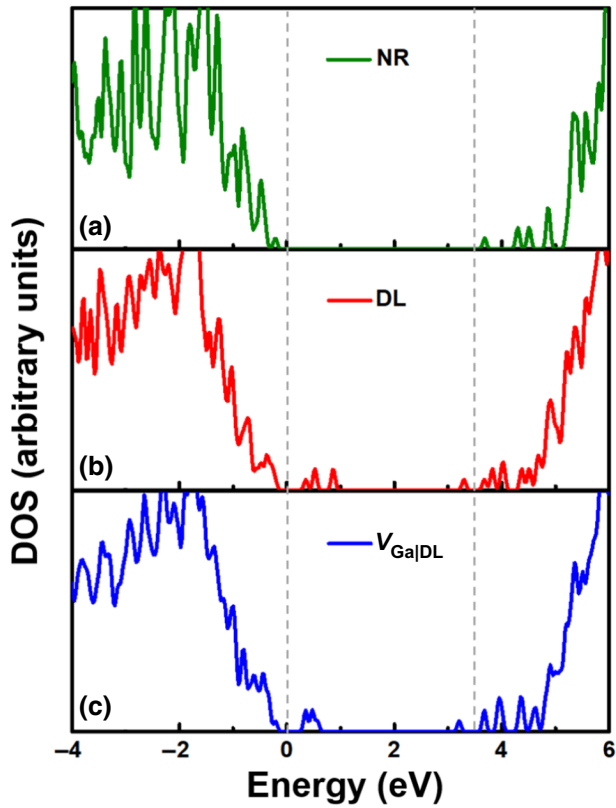
FIG. 2. Density of states (DOS) for (a) the pure GaN nanorod (NR), (b) the GaN nanorod containing a pure dislocation (DL), and (c) the GaN nanorod containing the V_{Ga}-decorated dislocation ($V_{Ga|DL}$).
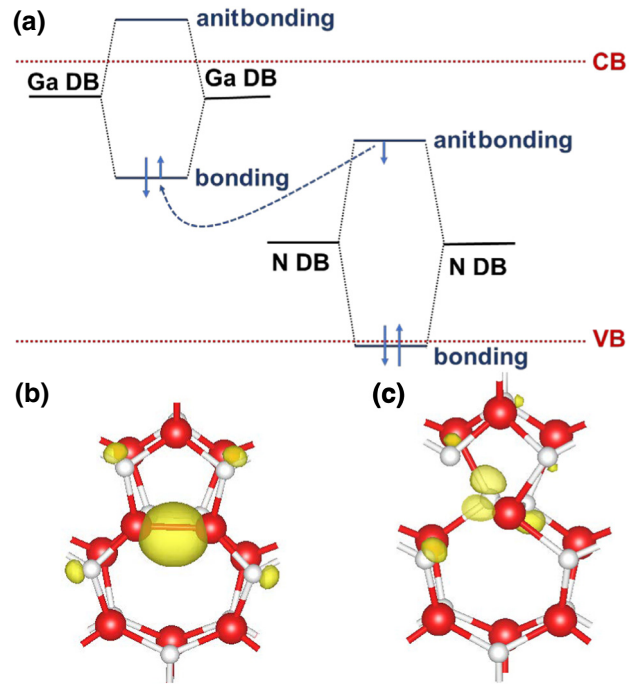

FIG. 3. (a) Electron transfer and formation of the deep state of the 5-7-atom-ring-core threading dislocation. Charge density isosurfaces of occupied deep levels above the VBM of the GaN nanorod containing (b) the pure 5-7-atom-ring-core threading dislocation and (c) the V_{Ga}-decorated dislocation. CB, conduction band; DB, dangling bond; VB, valence band.

interact with acceptors owning partially occupied or unoccupied states by electron transfer. The most common acceptor in undoped GaN is the Ga vacancy (V_{Ga}) because of the unintentional n-type doping [27,28]. Therefore, we focus on the electronic interaction between the threading dislocation and V_{Ga}. The structure of the V_{Ga}-decorated dislocation is constructed by removing one of the Ga atoms of the Ga-Ga dimer at the dislocation core. As shown in Fig. 3(c), the remaining Ga atom relaxes toward the dislocation core on structural relaxation. The decoration energy (E_d) of V_{Ga} at the threading dislocation core is calculated by

$$E_d = E_t(V_{Ga|DL}) - E_t(V_{Ga|perf}), \qquad (1)$$

where $E_t(V_{Ga|DL})$ and $E_t(V_{Ga|perf})$ are the total energies of V_{Ga} formed at the dislocation core and in the perfect region away from the dislocation. The definition of the decoration energy is similar to the definition of the segregation energy of point defects at the grain boundaries in polycrystalline semiconductors [29]. The negative segregation energy indicates that point defects will spontaneously segregate at grain boundaries. In this case, the strongly negative decoration energy of -4.65 eV indicates

that V_{Ga} will spontaneously form at the core of threading dislocations during its formation. As shown in Fig. 2(c), for the defect states above the VBM, the deeper states disappear and the shallower states shift slightly toward the VBM of GaN on V_{Ga} decoration. This moves the deep level of the threading dislocation to shallower positions in the band gap of GaN, which may constructively contribute to the dislocation tolerance of GaN devices. We also calculate the charge-density isosurfaces of the occupied states above the VBM for GaN containing V_{Ga}-decorated threading dislocations. As shown in Fig. 3(c), V_{Ga} and the N-N dimer at the dislocation core mostly contribute to the occupied states above the VBM.

In addition to the shift of detrimental deep electronic states toward the VBM on V_{Ga} decoration, the position of unoccupied states below the CBM shifts slightly to lower energies in the band gap of GaN [Fig. 2(c)]. As a result, there emerge two distinct electron-transfer channels: one through the pure dislocation state and the other through the V_{Ga}-decorated dislocation state below the CBM.

B. Properties of dislocations in (Al, Ga)N alloys

The electronic properties of threading dislocations in (Al, Ga)N alloys can be derived from the shifts of the band edge and defect states with respect to those of
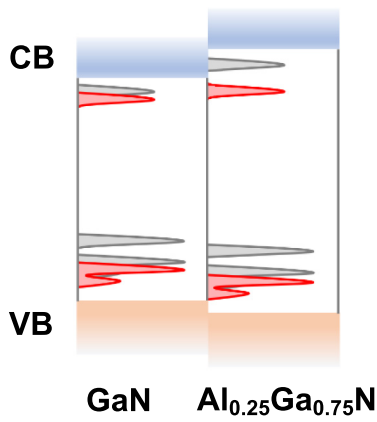
FIG. 4. Physical derivation of electronic properties of dislocations in $Al_{0.25}Ga_{0.75}N$. Electronic states of pure and V_{III}-decorated dislocations are denoted by gray and red regions, respectively. CB, conduction band; VB, valence band.

GaN. In $(Al,Ga)N/GaN$ heterostructures, the Al content is usually in the range of 20%–30%. Therefore, we take $Al_{0.25}Ga_{0.75}N$ as an example to illustrate the physical derivation of the electronic properties of dislocations in $(Al,Ga)N$ alloys.

The band edges of $Al_{0.25}Ga_{0.75}N$ are calculated by the linear interpolation from the band offsets of GaN and AlN [30]. As shown in Fig. 4, when the Al content increases, the increase of the CBM is greater than the decrease of the VBM. In $Al_{0.25}Ga_{0.75}N$, Al and Ga vacancies (V_{III}) share similar defect properties and dominate the configurations of acceptors in $Al_{0.25}Ga_{0.75}N$ [31]. The interaction between the threading dislocation and V_{III} in $Al_{0.25}Ga_{0.75}N$ is similar to that in GaN. When the composition of a semiconductor-alloy changes, the shallow defect levels shift with respect to the band edges by similar degrees, while deep levels tend to line up and remain in the midgap [32,33]. For the defect states of threading dislocations below the CBM, the defect states of the pure dislocation are shallower than that of the V_{III}-decorated dislocation. Therefore, when the host changes from GaN to $Al_{0.25}Ga_{0.75}N$, the states of the pure threading dislocation tend to shift with the CBM, while the states of the V_{III}-decorated dislocation are more inclined to line up with those in GaN. For the defect states above the VBM, the states of the V_{III}-decorated dislocation are shallower. Therefore, the shift of states of the V_{III}-decorated dislocation above the VBM is severer than that of the pure dislocation (Fig. 4).

It is clear that the V_{III}-decoration also gives rise to the dislocation tolerance of $(Al,Ga)N$ alloys because of the shallower defect states above the VBM for V_{III}-decorated dislocations. For the dislocation states below the CBM, both the defect states of V_{III}-decorated dislocations and those of pure dislocations can serve as electron-transfer

channels in $(Al,Ga)N$. These two electron-transfer channels could induce distinct FP emission in $(Al,Ga)N/GaN$ devices, which can be directly observed in experimental I-V measurements.

C. *I*-*V* measurements of (Al, Ga)N/GaN Schottky diodes

In experiments, $(Al,Ga)N/GaN$ heterostructures on (0001)-oriented sapphire substrates are grown by metal-organic chemical vapor deposition. The structure consists of a 21-nm undoped $(Al,Ga)N$ barrier layer and a 2-μm undoped GaN buffer layer. The Al content of the $(Al,Ga)N$ layer is estimated to be 26%. During the fabrication of $(Al,Ga)N/GaN$ Schottky diodes, a device mesa was formed by Cl_2 and BCl_3 plasma dry etching in an inductively-coupled-plasma reactive ion etching (ICP-RIE) system. The source and drain Ohmic contacts are formed by deposition of Ti/Al/Ti/Au annealed at 870 °C for 45 s. The Schottky contact is formed by Ni/Au electron-beam evaporation and lift-off. Temperature-dependent I-V measurements are performed with an Agilent B1500 semiconductor parameter analyzer in the temperature range from 298 to 418 K.

Figure 5(a) shows the current of $(Al,Ga)N/GaN$ Schottky diodes as a function of the bias voltage at temperatures ranging from 298 to 418 K. For $(Al,Ga)N/GaN$ Schottky diodes under the reverse voltage, the emission mechanism commonly includes FP emission, trap-assisted tunneling (TAT), and Fowler-Nordheim tunneling (FNT) [34]. FNT usually occurs in reverse-biased diodes below 150 K. Moreover, the current dominated by TAT or FNT is independent of the temperature [35]. In contrast, FP emission originates from the transfer of electrons from the Schottky metal into a continuum dislocation state of the barrier enhanced by the electronic field, which is strongly temperature dependent [36,37]. As shown in Fig. 5(a), the current of $(Al,Ga)N/GaN$ Schottky diodes exhibits an obvious temperature dependence. Therefore, we consider that the FP emission dominates the mechanism of current for $(Al,Ga)N/GaN$ Schottky diodes under the reverse voltage. The FP current is given by [38,39]

$$I_{FP} = CE_b A \exp\left[-\frac{q(\phi_t - \sqrt{qE_b/\pi\varepsilon_0\varepsilon_s})}{k_B T} \right], \quad (2)$$

where E_b is the electric field in the $(Al,Ga)N$ barrier at the metal-semiconductor interface, ϕ_t is the barrier height of electron emission from the Schottky metal to the continuum dislocation state, ε_0 is the permittivity of free space, ε_s is the relative dielectric permittivity at high frequency, and k_B is the Boltzmann constant. Taking logarithms of Eq. (2), we have,

$$\log_{10}(I_{FP}/E_b) = \log_{10} C + \log_{10} A + \frac{q}{k_B T}\sqrt{\frac{qE_b}{\pi\varepsilon_0\varepsilon_s}} - \frac{q\phi_t}{k_B T}$$
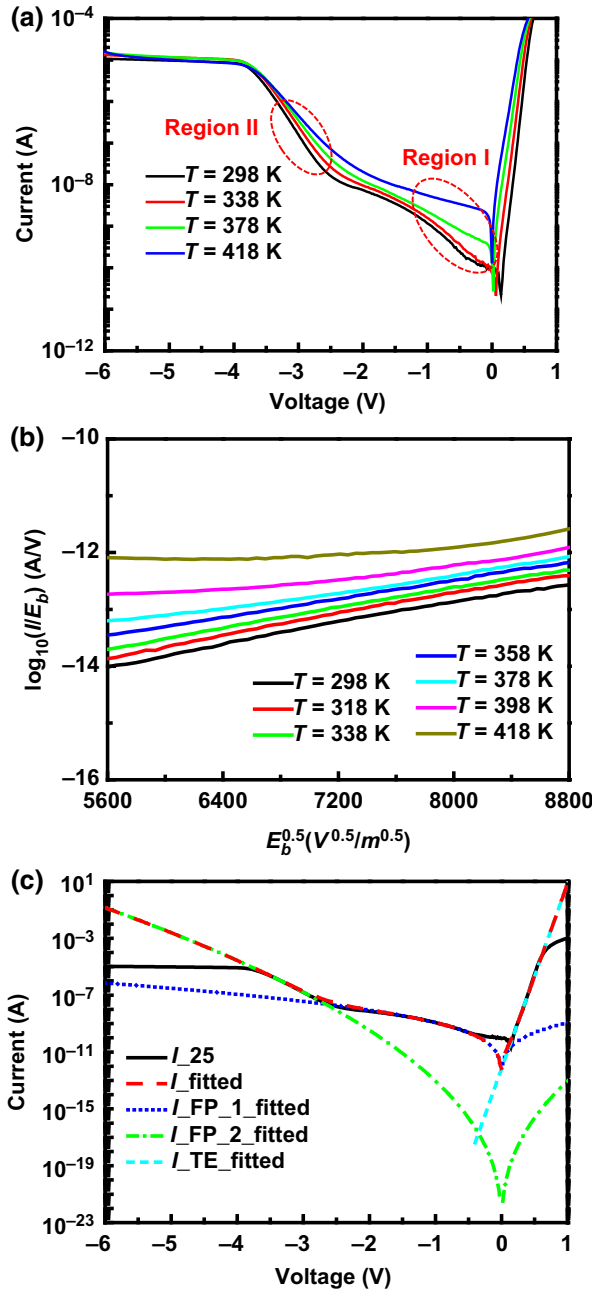
FIG. 5. (a) Current of the (Al, Ga)N/GaN Schottky diode as a function of voltage at temperatures ranging from 298 to 418 K. (b) Measured $\log_{10}(I/E_b)$ as a function of $\sqrt{E_b}$ at temperatures ranging from 298 to 418 K. (c) Measured and fitted curves of the current of a (Al, Ga)N/GaN Schottky diode as a function of bias voltage at 298 K.

$$\equiv s(T)\sqrt{E_b} + i(T), \qquad (3)$$

where $s(T) = (q/k_B T)\sqrt{(q/\pi \varepsilon_0 \varepsilon_s)}$ and $i(T) = \log_{10} C + \log_{10} A - (q\phi_t/k_B T)$ represent the slope and intercept of the curve of $\log_{10}(I_{FP}/E_b)$ versus $\sqrt{E_b}$, respectively. We can see from Eq. (3) that for the FP-emission-dominated current of (Al, Ga)N/GaN Schottky diodes, $\log_{10}(I_{FP}/E_b)$

should vary linearly with $\sqrt{E_b}$. The experimental results are shown in Fig. 5(b). It is clearly seen that the measured $\log_{10}(I/E_b)$ exhibits a linear dependence with respect to $\sqrt{E_b}$ from 298 to 378 K. Moreover, the current increases rapidly with increasing temperature. This verifies the dominant role of the FP emission for the reverse-biased (Al, Ga)N/GaN Schottky diodes in our experiments. The slight deviation of $\log_{10}(I_{PF}/E_b)$ from the linear dependence on $\sqrt{E_b}$ at 398 and 418 K is due to the thermionic emission (TE) involved at high temperatures. In general, the FP emission exhibits both temperature and voltage dependence of the current. In Fig. 5(a), one can see two distinct regions (regions I and II) with different temperature and voltage dependences of the current, which indicates the existence of two distinct FP-emission states.

Next, we quantitatively describe the current-transport mechanism of (Al, Ga)N/GaN Schottky diodes. For the current under the reverse voltage, we fit the measured $\log_{10}(I/E_b)$as a function of $\sqrt{E_b}$ with Eq. (3) to estimate the barrier heights of these two FP-emission states (ϕ_t). From the slopes of $i(T)$ versus $1/T$, we obtain barrier heights of 0.47 and 1.07 eV for the electron emission from the Schottky metal to the dislocation states of the (Al, Ga)N barrier. With the fitted values, we calculate the total fitted current of (Al, Ga)N/GaN Schottky diodes by

$$I_{\text{fitted}} = I_{FP\_1} + I_{FP\_2} \qquad (4)$$

As shown in Fig. 5(c), the fitted current coincides well with the measured current. This verifies the fact that the two-state FP emission dominants the current transport of reverse-biased (Al, Ga)N/GaN Schottky diodes.

Finally, we discuss the effect of acceptor decoration of threading dislocations on the device performance of (Al, Ga)N/GaN Schottky diodes. On the basis of the experimental results that (i) the current of reverse-biased (Al, Ga)N/GaN Schottky diodes exhibits both voltage and temperature dependence, (ii) after the fitting of the current of reverse-biased (Al, Ga)N/GaN Schottky diodes with the FP model, the logarithm of the current density divided by the applied electric field [$\log_{10}(I_{PF}/E_b)$] exhibits a linear dependence on the square root of the field ($\sqrt{E_b}$), and (iii) the fitted current ($I_{FP\_1} + I_{FP\_2}$) coincides well with the measured reverse current leakage, we conclude that the two-state FP emission well describes the current of reverse-biased (Al, Ga)N/GaN Schottky diodes. Since the FP emission originates from the transport of electrons via the continuum dislocation state, the observation of the two-state FP emission should correspond to two distinct dislocation states in the (Al, Ga)N barrier. According to the above first-principles prediction and analysis, these two dislocation states could be the pure dislocation state and the V_{III}-decorated dislocation state. For (Al, Ga)N/GaN Schottky diodes under the reverse voltage, electrons firstly transfer along the low-energy V_{III}-decorated dislocation
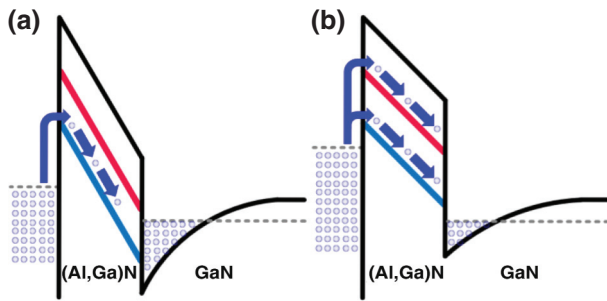
FIG. 6. FP emissions via (a) a V_{III}-decorated dislocation state and (b) a pure dislocation state.

level [Fig. 6(a)]. As the reverse voltage increases, electrons in the conducting V_{III}-decorated dislocation state become saturated. When the excess electrons gain sufficient energy with the increasing reverse voltage, the electrons begin to transfer along the pure dislocation state [Fig. 6(b)]. This intuitive physical picture bridges the distinct electron-transfer channels in $(Al, Ga)N$ and the two FP-emission behaviors observed in $(Al, Ga)N/GaN$ heterostructures.

IV. CONCLUSION

In conclusion, we demonstrate that the threading dislocations in $(Al, Ga)N/GaN$ heterostructures can be spontaneously decorated by acceptors. On one hand, the acceptor decoration shifts the detrimental deep states of threading dislocations above the VBM to shallower positions in the band gap of GaN, which may constructively contribute to the dislocation tolerance of GaN devices. On the other hand, the acceptor-decorated dislocation state near the CBM provides an additional electron-transfer channel besides that through the pure threading dislocations. These two distinct electron-transfer channels result in two-state FP emission for reverse-biased $(Al, Ga)N/GaN$ Schottky diodes.

[1] J. Zuniga-Perez, V. Consonni, L. Lymperakis, X. Kong, A. Trampert, S. Fernandez-Garrido, O. Brandt, H. Renevier, S. Keller, K. Hestroffer, and M. R. Wagner, Polarity in GaN and ZnO: Theory, measurement, growth, and devices, Appl. Phys. Rev. **3**, 041303 (2016).

[2] J. Millán, P. Godignon, X. Perpiñà, A. Pérez-Tomás, and J. Rebollo, A survey of wide bandgap power semiconductor devices, IEEE Trans. Power Electron. **29**, 2155 (2014).

[3] A. Dadgar and M. Weyers, in *Metalorganic Vapor Phase Epitaxy (MOVPE): Growth, Materials Properties, and Applications*, edited by Stuart Irvine and Peter Capper (John Wiley & Sons, West Sussex, 2019), p. 109.

[4] S. J. Pearton, J. C. Zolper, R. J. Shul, and F. Ren, Gan: Processing, defects, and devices, J. Appl. Phys. **86**, 1 (1999).

[5] M. A. Reshchikov and H. Morkoç, Luminescence properties of defects in GaN, J. Appl. Phys. **97**, 061301 (2005).

[6] L. Zhang, W. E. McMahon, and S.-H. Wei, Passivation of deep electronic states of partial dislocations in GaAs: A theoretical study, Appl. Phys. Lett. **96**, 121912 (2010).

[7] J.-S. Park, B. Huang, S.-H. Wei, J. Kang, and W. E. McMahon, Period-doubling reconstructions of semiconductor partial dislocations, NPG Asia Mater. **7**, e216 (2015).

[8] N. G. Weimann, L. F. Eastman, D. Doppalapudi, H. M. Ng, and T. D. Moustakas, Scattering of electrons at threading dislocations in GaN, J. Appl. Phys. **83**, 3656 (1998).

[9] R. Quary, *Gallium Nitride Electronics*, editd by R. Hull, R. M. Osgood, Jr. J. Parisi, and H. Warlimont (Springer, Freiburg, 2008).

[10] S. M. Islam, K. Lee, J. Verma, V. Protasenko, S. Rouvimov, S. Bharadwaj, h. Xing, and D. Jena, MBE-grown 232–270 nm deep-UV LEDs using monolayer thin binary GaN/AlN quantum heterostructures, Appl. Phys. Lett. **110**, 041108 (2017).

[11] S. Li, Z. Fang, H. Chen, J. Li, X. Chen, X. Yuan, T. Sekiguchi, Q. Wang, and J. Kang, Defect influence on luminescence efficiency of GaN-based LEDs, Mater. Sci. Semicon. Pro. **9**, 371 (2006).

[12] I. Belabbas, A. Béré, J. Chen, S. Petit, M. A. Belkhir, P. Ruterana, and G. Nouet, Atomistic modeling of the(a+c)-mixed dislocation core in wurtzite GaN, Phys. Rev. B **75**, 11 (2007).

[13] F. C.-P. Massabuau, S. L. Rhode, M. K. Horton, T. J. O'Hanlon, A. Kovács, M. S. Zielinski, M. J. Kappers, R. E. Dunin-Borkowski, C. J. Humphreys, and R. A. Oliver, Dislocations in $(Al, Ga)N$: Core structure, atom segregation, and optical properties, Nano Lett. **17**, 4846 (2017).

[14] S. Besendörfer, E. Meissner, A. Lesnik, J. Friedrich, A. Dadgar, and T. Erlbacher, Methodology for the investigation of threading dislocations as a source of vertical leakage in $(Al, Ga)N/GaN$-HEMT heterostructures for power devices, J. Appl. Phys. **125**, 095704 (2019).

[15] I. Belabbas, P. Ruterana, J. Chen, and G. Nouet, The atomic and electronic structure of dislocations in Ga-based nitride semiconductors, Philos. Mag. **86**, 2241 (2006).

[16] J. Elsner, R. Jones, P. K. Sitch, V. D. Porezag, M. Elstner, T. Frauenheim, M. I. Heggie, S. Öberg, and P. R. Briddon, Theory of Threading Edge and Screw Dislocations in GaN, Phys. Rev. Lett. **79**, 3672 (1997).

[17] A. F. Wright and J. Furthmüller, Theoretical investigation of edge dislocations in AlN, Appl. Phys. Lett. **72**, 3467 (1998).

[18] R. Gröger, L. Leconte, and A. Ostapovets, Structure and stability of threading edge and screw dislocations in bulk GaN, Comput. Mater. Sci. **99**, 195 (2015).

[19] L. Lymperakis, J. Neugebauer, M. Albrecht, T. Remmele, and H. P. Strunk, Strain Induced Deep Electronic States Around Threading Dislocations in GaN, Phys. Rev. Lett. **93**, 196401 (2004).

[20] S. Christenson, W. Xie, Y.-Y. Sun, and S. B. Zhang, Kinetic path towards the passivation of threading dislocations in GaN by oxygen impurities, Phys. Rev. B **95**, 121201(R) (2017).

[21] Y. Gai, J. Li, S. Li, J. Xia, Y. Yan, and S.-H. Wei, Design of shallow acceptors in ZnO through compensated donor-cceptor complexes: A density functional calculation, Phys. Rev. B **80**, 153201 (2009).

[22] D. Segev and S.-H. Wei, Design of Shallow Donor Levels in Diamond by Isovalent-Donor Coupling, Phys. Rev. Lett. **91**, 126406 (2003).

[23] P. E. Blöchl, Projector augmented-wave method, Phys. Rev. B **50**, 17953 (1994).

[24] J. F. G. Kresse, Efficient iterative schemes for ab initio total-energy calculations using a plane-wave basis set, Phys. Rev. B **54**, 11169 (1996).

[25] J. Heyd, G. E. Scuseria, and M. Ernzerhof, Hybrid functionals based on a screened Coulomb potential, J. Chem. Phys. **118**, 8207 (2003).

[26] H. J. Monkhorst and J. D. Pack, Special points for Brillouin-zone integrations, Phys. Rev. B **13**, 5188 (1976).

[27] J. L. Lyons and C. G. Van de Walle, Computationally predicted energies and properties of defects in GaN, NPJ Comput. Mater. **3**, 1 (2017).

[28] K. Laaksonen, M. G. Ganchenkova, and R. M. Nieminen, Vacancies in wurtzite GaN and AlN, J. Phys. Condens. Matter. **21**, 015803 (2009).

[29] Y. Yan, C.-S. Jiang, R. Noufi, S.-H. Wei, H. R. Moutinho, and M. M. Al-Jassim, Electrically Benign Behavior of Grain Boundaries in Polycrystalline $CuInSe_2$ Films, Phys. Rev. Lett. **99**, 235504 (2007).

[30] S.-H. Wei and A. Zunger, Valence band splittings and band offsets of AlN, GaN, and InN, Appl. Phys. Lett. **69**, 2719 (1996).

[31] R. Wang, X. Tong, J. Xu, S. Zhang, P. Zheng, F. Chen, and W. Tan, Assessing the Role of Fluorine in the Performance of $Al_xGa_{1-x}N$/GaN High-Electron-Mobility Transistors From First-Principles Calculations, Phys. Rev. Appl. **11**, 054021 (2019).

[32] R. Wang, W. Tan, J. Zhang, F.-X. Chen, and S.-H. Wei, First-principles study of alloying effects on fluorine incorporation in $Al_xGa_{1-x}N$ alloys, J. Phys. D: Appl. Phys. **51**, 065108 (2018).

[33] B. Huang, M. Yoon, B. G. Sumpter, S.-H. Wei, and F. Liu, Alloy Engineering of Defect Properties in Semiconductors: Suppression of Deep Levels in Transition-Metal Dichalcogenides, Phys. Rev. Lett. **115**, 126806 (2015).

[34] H. Zhang, E. J. Miller, and E. T. Yu, Analysis of leakage current mechanisms in schottky contacts to GaN and $Al_{0.25}Ga_{0.75}$N/GaN grown by molecular-beam epitaxy, J. Appl. Phys. **99**, 023703 (2006).

[35] S. Turuvekere, N. Karumuri, A. A. Rahman, A. Bhattacharya, A. DasGupta, and N. DasGupta, Gate leakage mechanisms in (Al, Ga)N/GaN and AlInN/GaN HEMTs: Comparison and modeling, IEEE Trans. Elec. Dev. **60**, 3157 (2013).

[36] E. J. Miller, D. M. Schaadt, E. T. Yua, X. L. Sun, L. J. Brillson, P. Waltereit, and J. S. Speck, Origin and microscopic mechanism for suppression of leakage currents in schottky contacts to GaN grown by molecular-beam epitaxy, J. Appl. Phys. **94**, 7611 (2003).

[37] W. Chikhaoui, J.-M. Bluet, M.-A. Poisson, N. Sarazin, C. Dua, and C. Bru-Chevallier, Current deep level transient spectroscopy analysis of AlInN/GaN high electron mobility transistors: Mechanism of gate leakage, Appl. Phys. Lett **96**, 072107 (2010).

[38] O. Mitrofanov and M. Manfra, Poole-Frenkel electron emission from the traps in (Al, Ga)N/GaN transistors, J. Appl. Phys. **95**, 6414 (2004).

[39] E. Arslan, S. Bütün, and E. Ozbay, Leakage current by frenkel–poole emission in Ni/Au schottky contacts on $Al_{0.83}In_{0.17}$N/AlN/GaN heterostructures, Appl. Phys. Lett. **94**, 142106 (2009).